Supplement of Hydrol. Earth Syst. Sci., 29, 5493–5513, 2025 https://doi.org/10.5194/hess-29-5493-2025-supplement © Author(s) 2025. CC BY 4.0 License.





Supplement of

Controls on spatial and temporal variability of soil moisture across a heterogeneous boreal forest landscape

Francesco Zignol et al.

Correspondence to: Francesco Zignol (francesco.zignol@slu.se)

The copyright of individual parts of the supplement might differ from the article licence.

DESCRIPTION OF SOIL MOISTURE PREDICTORS

This section contains a detailed description of all the variables that were evaluated in this study. Variables are listed in the same order as those in Table 1 and Table 2 of the main manuscript.

S1. Spatial predictors (refer to Table 1 in the main manuscript)

These variables were used to predict spatial variability in soil moisture. For clarity, they were organized into four broad groups: soil, topography, vegetation, and land use/land cover (LULC).

S1.1 Soil

■ Organic layer thickness (olt)

This variable represents the depth of the organic layer, defined as the distance from the surface to the top of the mineral soil. We determined it using a measuring stick at the exact locations where the dataloggers were placed during the field campaign in June/July 2022. Measured values ranged between 0 and 92 cm. Additionally, the value 99 was used to indicate peat soils thicker than 1 m.

SGU soil depth map (sd-sgu)

The SGU soil depth map is a 10×10 m resolution grid that estimates soil depth to bedrock across Sweden. It was developed by the Swedish Geological Survey (SGU), using an interpolation method based on soil depth observations from drilling and other geological surveys (SGU, 2024a). The model incorporates ancillary data such as fracture zones and soil type classifications to improve accuracy. However, uncertainty increases with distance from observation points, especially when measurements are sparse, exceeding several hundred meters. The model is updated at least once a year, with continuous integration of new soil depth observations from various SGU databases. Values at the datalogger locations in Krycklan ranged from 0 to 33 m below surface.

■ Soil moisture survey (sms)

Soil moisture was classified in the field according to the Swedish National Forest Inventory (NFI) protocol during the autumn of 2014 and the spring of 2015 (Larson et al., 2022). Following this protocol (SLU, 2021a), we estimated each plot's average groundwater table depth as a function of its landscape position, vegetation patterns, and soil type. This classification is independent of seasonal variations in soil moisture, and provides an indicator of the averaged soil moisture conditions within each plot. The 78 plots were assigned to one of five categories: dry, mesic, mesic-moist, moist, and wet.

- Dry soils have a groundwater table more than 2 m below the surface, typically found on hilltops, ridges, and eskers. These areas are usually characterized by coarse-textured soils, including Podzols, Arenosols, Regosols, or Leptosols.
- Mesic soils have a groundwater table between 1 and 2 m deep, with Podzol as the dominant soil type. A thin organic layer (4–10 cm) typically covers this surface, often supporting dryland mosses.

- Mesic-moist soils have a groundwater table less than 1 m deep, often located on flat ground in lower-lying areas that
 undergo seasonal wetting. Podzols are common, but have a thicker organic layer compared to mesic soils, usually
 covered by wetland mosses, with trees growing on humps.
- Moist soils have a groundwater table less than 1 m deep, with visible water in depressions. These soils, mainly
 Histosols, Regosols, or Gleysols, are found in low-lying terrain, such as the bases of slopes and flatlands. Wetland
 mosses dominate the vegetation, with trees typically growing on small mounds.
- Wet soils have a groundwater table at or just below the surface. They are commonly found in open peatlands, characterized by poor drainage and pools of standing water. The soil type is generally Histosol or Gleysol, and coniferous trees rarely form stands.

This ordinal data was then converted into numerical values (1 to 5) for analysis in the OPLS model, maintaining the original soil moisture gradient, with 1 representing dry soils and 5 representing wet soils.

■ Soil survey (ss)

Soil was classified in the field according to the Swedish Forest Soil Inventory (SFSI) protocol during the snowfree seasons of 2019 and 2020 (Larson et al., 2023). Following this protocol (SLU, 2021a), we first determined parent material and soil texture at predefined depths in the upper and lower parts of the soil profile within each plot. Then, we identified soil texture by feel analysis based on nine separate classes for each parent material (see table below).

Code	Sorted sediment	Till
1	Boulders/stones	Rocky/stony till
2	Gravel	Gravely till
3	Coarse sand	Sandy till
4	Medium sand	Sandy-silty till
5	Fine sand	Silty-sandy till
6	Coarse silt	Coarse silty till
7	Fine silt	Fine silty till
8	Clay	Clayey till
9	Peat	Peat

Each soil profile was finally classified according to the World Reference Base of Soil Resources (IUSS and FAO, 2015). Five soil types were identified at the locations of the dataloggers used in this study:

- Loamy sand (ss-losa): a coarse-textured soil with a high proportion of sand and just enough silt and clay to slightly
 improve moisture retention and structure.
- Peat (ss-pt): an organic-rich soil composed largely of decomposed plant material, characterized by high water retention and low bulk density.
- Sand (ss-sa): a soil dominated by large mineral particles, offering excellent drainage but low nutrient and water-holding capacity.

- Sandy loam (ss-salo): a moderately coarse soil with a balanced mix of sand, silt, and a small amount of clay, providing better fertility and moisture retention than pure sand.
- Silt loam (ss-silo): a fine-textured soil with a high silt content, known for its smooth feel, good fertility, and moderate water-holding capacity.

■ SGU Quaternary deposit map (st)

The SGU Quaternary deposit map illustrates the distribution and characteristics of soil types across Sweden, focusing on deposits formed during the Quaternary period (SGU, 2024b). It classifies surface and near-surface sediments based on their composition and genesis, providing information on landforms, boulders, and glacial features. Six soil types were identified at the locations of the dataloggers used in this study (Fig. S1a):

- Clay to silt (st-cs, code: 86): fine-grained sediments deposited by meltwater in calm glacial lakes and marine basins, typically accumulating in lowland areas and topographic depressions sheltered from wave and current activity.
- Glacifluvial sediment (st-gfs, code: 50): sorted sand and gravel deposited by meltwater streams flowing from glaciers during deglaciation.
- Postglacial sand (st-ps, code: 31): sandy sediments redeposited by wave and current action during land uplift after the
 last glaciation, often found in coastal or formerly submerged areas below the highest coastline.
- Postglacial sand to gravel (st-psg, code: 84): coarse-grained sediments shaped by postglacial wave erosion and redeposition, commonly occurring around ridges below the highest coastline and in areas exposed to strong shoreline processes.
- Peat (st-pt, code: 75): organic-rich soil formed in water-saturated, low-oxygen environments where shallow
 groundwater tables and poor drainage prevent full decomposition of plant material. Often beginning in low-lying
 areas or former glacial lakes after deglaciation, peatlands, especially in northern Sweden, can gradually expand and
 even grow upslope, forming extensive bogs and marshes.
- Till (st-till, code: 100): unsorted glacial sediment composed of clay, silt, sand, gravel, and boulders, originally eroded from the bedrock or older soils and then deposited by moving ice.

These classes were derived by combining two layers: "jg2", representing the soil substrate at about 0.5 m below the surface, and "jy1", a thin and discontinuous layer of soil closer to the surface. The 1:25,000 scale of the map was achieved through extensive field surveys, image interpretation, and the use of high-resolution digital elevation models (DEMs).

S1.2 Topography

S1.2.1 Topographic indices

To characterize topographic features, we calculated nine indices based on a digital elevation model (DEM) derived from an airborne LiDAR scan conducted in 2015. The initial DEM (Fig. S1b), with a 0.5×0.5 m resolution, was generated from a point cloud with a density of 10 points per square meter. It had horizontal and vertical accuracies of 0.1 m and 0.3 m, respectively.

To evaluate the effects of spatial resolution, the DEM was resampled to coarser grids of 1, 2, 4, 8, 16, 32, and 64 m. Before calculating the indices, each DEM was preprocessed for hydrological accuracy using the two-step breaching approach proposed by Lidberg et al. (2017). This method first involves carving a short path into the DEM at locations where culverts and mapped streams intersect road embankments, followed by resolving remaining depressions using the complete breaching tool in Whitebox Tools (Lindsay, 2016). The nine topographic indices described below were then computed for all eight spatial resolutions using mostly Whitebox Tools (Lindsay, 2016b) or, when indicated, ArcGIS Pro (Esri Inc., 2023).

■ Depth to water (dtw)

The depth to water (dtw) index (Murphy et al., 2008) predicts soil moisture by estimating the least-cost path from any cell in the landscape to the nearest surface water cell (i.e., stream network with dtw = 0). It accounts for vertical and horizontal distances between cells as well as for cell size and orientation, and can be expressed as follows:

$$DTW = \left[\sum \frac{dz_i}{dx_i} a\right] x_c , \qquad (S1)$$

where dz_i and dx_i represent the vertical and horizontal distances between pairs of cells, the constant α can assume either value equal to 1 (when two cells share a common side – parallel adjacency) or $\sqrt{2}$ (when they only share a common vertex – diagonal adjacency), and x_c is the size of the cells. Cells farther away or higher from the flow channels have higher dtw values, indicating drier conditions. The stream network, including a flow pointer grid and a flow accumulation grid, was extracted using the multiple flow direction algorithm (MD ∞) (Seibert and McGlynn, 2007). In addition to the eight DEM spatial resolutions, this index was calculated for six stream initiation thresholds of 1, 2, 4, 8, 16, and 32 ha, resulting in 48 layers.

■ Diffuse solar radiation (dfr)

This parameter represents the diffuse incoming solar radiation (dfr), measured in watt-hours per square meter (Wh/m²). It was calculated using the ArcGIS tool "Area Solar Radiation", based on topography (elevation, slope, and aspect) for the entire study period (July 5 – October 4, 2022). The model was configured with a sky size of 200 cells for the viewshed, sky map, and sun map. It used 8 zenith divisions and 8 azimuth divisions, with 32 azimuth directions for the viewshed calculation. The diffuse radiation model followed a standard overcast sky configuration, where the diffuse radiation flux varies with the zenith angle. Additionally, we assumed generally clear sky conditions throughout the study period, setting the fraction of diffuse radiation flux to 0.3 and atmospheric transmittance (the fraction of radiation that passes through the atmosphere) to 0.5. This index was calculated for each of the eight DEM spatial resolutions.

Direct solar radiation (drr)

This parameter represents the direct incoming solar radiation in watt-hours per square meter (Wh/m²). It was generated along with diffuse solar radiation using the same method and model parameters, and computed for the eight DEM spatial resolutions.

■ <u>Downslope index (di)</u>

The downslope index (di) indicates the length of a flow path required to descend a given vertical distance d (m) along the steepest direction (Hjerdt et al., 2004). It can be reported either as a distance, L_d , or as a gradient, $\tan \alpha_d$, calculated as:

$$\tan \alpha_d = \frac{d}{L_d},\tag{S2}$$

where L_d is the horizontal distance to the point that is d m below the elevation of the starting cell, following the steepest-direction flow path. In addition to the eight DEM spatial resolutions, the downslope index was calculated for vertical distances of 2 m and 4 m, resulting in 16 layers.

■ Elevation above stream (eas)

The elevation above stream (eas) index (Rennó et al., 2008) estimates soil moisture by measuring the elevation difference between any cell in the landscape and the nearest surface water cell along the downslope flow path. This path is determined using a flow pointer grid obtained using the multiple flow direction algorithm (MD ∞) (Seibert and McGlynn, 2007). In addition to the eight DEM spatial resolutions, this index was calculated for six stream initiation thresholds of 1, 2, 4, 8, 16, and 32 ha, vielding a total of 48 layers.

■ Landscape wetness index (wilt)

The wetness index based on landscape position and topography (wilt), simply called landscape wetness index in our paper, is a modification of the more common topographic wetness index (twi, described below) to reflect landscape position and better predict soil moisture in landscapes with dominant groundwater flow (Meles et al., 2020). It is expressed as follows:

$$WILT = ln\left(\frac{A}{\Delta X \times \Delta Z \times tan \beta}\right),\tag{S3}$$

where A is the upslope contributing area calculated using the D-infinity flow routing algorithm (D ∞) (Tarboton, 1997), ΔX is the horizontal distance from the nearest surface water feature, ΔZ is the depth to groundwater, and β is the local slope of the grid cells in degrees. This index was computed for each of the eight DEM spatial resolutions.

■ Plan curvature (plc)

Plan curvature (plc) refers to the curvature of the surface perpendicular to the direction of the maximum slope (Wilson and Gallant, 2000). This index allows distinguishing between areas where slopes converge or diverge. Specifically, positive values of plan curvature indicate concave, convergent areas where water and material tend to accumulate, such as valleys and drainage channels. In contrast, negative values represent convex, divergent areas, such as ridges and crests, where flow tends to disperse. Plan curvature was calculated for each of the eight DEM spatial resolutions.

Relative topographic position (rtp)

Relative topographic position (rtp) quantifies the elevation of a specific point relative to its surrounding terrain, providing insights into local topographic variation (Newman et al., 2018). Given a user-specified local neighborhood size, this index is calculated as follows:

$$RTP = \begin{cases} \frac{(z_0 - \mu)}{(\mu - z_{\min})}, & \text{if } z_0 < \mu \\ \frac{(z_0 - \mu)}{(z_{\max} - \mu)}, & \text{if } z_0 > \mu \end{cases}$$
(S4)

where z_0 is the elevation of the central cell, while z_{max} , z_{min} , and μ represent the maximum, minimum, and mean elevations within the local neighborhood, respectively. This index ranges from -1 to 1, indicating whether the central cell lies below or above the neighborhood mean. Positive values correspond to elevated landscape features, such as dry ridges, whereas negative values indicate low-lying, wetter areas, such as valleys. Relative topographic position was calculated for each of the eight DEM spatial resolutions.

■ Topographic wetness index (twi)

The topographic wetness index (twi) quantifies the spatial distribution of soil moisture by considering both the contributing upslope area and the local slope, where higher values indicate areas more prone to water accumulation and saturation (Beven and Kirkby, 1979). It is expressed as follows:

$$TWI = ln\left(\frac{\alpha}{\tan \beta}\right),\tag{S5}$$

where α is the upslope source area calculated using the D-infinity flow routing algorithm (D ∞) (Tarboton, 1997) and β is the local slope of the grid cells in degrees. This index was computed for each of the eight DEM spatial resolutions.

S1.2.1 Topography-based maps

In addition to the nine topographic indices described above, we also evaluated two national soil moisture maps that were obtained by combining multiple topographic indices and other secondary information, as specified below. We wanted to test their ability to explain soil moisture spatial variability compared to individual indices.

■ SLU soil moisture map (sm-slu)

Developed by the Swedish University of Agricultural Sciences (SLU), this map estimated soil moisture conditions across Sweden (Ågren et al., 2021). The majority of the variables used to generate the map, including several topographic indices and local topography measures, were calculated from a LiDAR-derived DEM at a 2 m resolution. To improve accuracy, the map was regionally adjusted by incorporating ancillary data on soil, geology, land use, and climate. The final product, evaluated in our analysis, is a wetness probability map ranging from 0% to 100% at a 2 m resolution (SLU, 2021b).

■ Soil moisture index map (smi)

This map was obtained from the National Land Cover Database of the Swedish Environmental Protection Agency (Naturvårdsverket, 2022). It is a weighted map that integrates the depth to water (dtw) index, described earlier, with the soil topographic wetness index (stwi), a modified version of the topographic wetness index (twi) that accounts for soil transmissivity estimated from quaternary deposit maps (Buchanan et al., 2014). It is expressed as follows:

$$SMI = \left(0.7 \times \frac{1}{DTW}\right) + \left(0.3 \times STWI\right). \tag{S6}$$

The spatial resolution of the soil moisture index map is 10×10 m.

S1.3 Vegetation

The vegetation data used in this study were either collected in the field or derived from remote sensing sources.

- Field data. With the exception of canopy openness (discussed below), field vegetation data were collected during a forest survey conducted in the late fall of 2019 and the early spring of 2020 based on a survey grid established in 2014 (Larson et al., 2023). This grid consists of 500 equally spaced plots (350 m apart) covering the entire Krycklan catchment. Within each 10 m radius plot, all trees with a diameter at breast height (DBH) (1.3 m) greater than 4 cm were surveyed. From this grid, we selected a subset of 78 plots instrumented with soil moisture dataloggers (section 2.2.1 in the main manuscript) (Figs. 1 and S1).
- Remote sensing data. Excluding the normalized difference vegetation index (discussed below), non-field vegetation data were extracted from the SLU Forest Map (SLU, 2010). Developed by the Swedish University of Agricultural Sciences (SLU), this map integrates field data from the Swedish National Forest Inventory (NFI) with satellite imagery from Landsat and SPOT sensors (Wallerman et al., 2021). Statistical modeling techniques were used to establish a relationship between ground-truth vegetation metrics from NFI and spectral data from the satellite images. These models were then applied across the satellite imagery to predict spatially continuous estimates of these vegetation metrics throughout Swedish forests. The SLU Forest Map has a spatial resolution of 25×25 m and was developed for the year 2010. While a more recent (2015) and more accurate (based on airborne laser scanning) version of this map is available for parts of Sweden, it does not cover the Krycklan catchment (Nilsson et al., 2017), so it couldn't be used for this study.

S1.3.1 Forest productivity

■ Biomass above ground (bio)

This variable represents the total dry mass of living plant material above the soil surface, including stem, branches, and foliage. We estimated biomass using species-specific allometric equations developed from empirical data collected across Sweden (Marklund, 1988). These equations relate tree biomass components to measurable tree parameters, primarily DBH and, in some cases, tree height, using logarithmic regression models. Separate equations were provided for different biomass fractions (stem, branch, foliage) and for each tree species commonly found in Swedish forests. The models were originally calibrated using destructive sampling of over 2,600 trees representing a wide range of sizes, species, and site conditions, ensuring broad applicability within Swedish forest types (Marklund, 1988). Biomass is expressed in tons of dry matter per hectare (ton/ha), with values across our 78 study plots ranging between about 15 and 370 ton/ha, except in clearcut areas, where biomass was set to 0. This variable was collected in the Krycklan forest survey 2019/2020.

■ <u>SLU forest biomass map (bio-slu)</u>

This variable represents the above-ground tree biomass density, measured in tons per hectare (ton/ha). Values refer to year 2010 and were extracted from a 25×25 m grid. Within our 78 study plots, bio-slu values ranged between 0 and 234 ton/ha.

■ Normalized difference vegetation index (ndvi)

This variable is a widely used indicator of vegetation health and forest productivity. NDVI is based on the difference in surface reflectance between the near infrared (*NIR*) and red (*Red*) bands, since healthy vegetation strongly reflects *NIR* light while absorbing *Red* light for photosynthesis. It is calculated as follows:

$$NDVI = \frac{NIR - Red}{NIR + Red}.$$
 (S7)

NDVI values range between -1 and 1, with negative values (-0.9 to -0.2) usually identifying water or very barren areas, values around zero (-0.2 to 0.2) representing bare soil or sparsely vegetated land, and positive values (0.2 to 0.7) generally showing increasingly healthy and dense vegetation or grass (Fig. S1c). We derived this index from two remote sensing sources: Landsat 8 (USGS, 2022) and Lantmäteriet Orthophoto (Lantmäteriet, 2021). Landsat 8 is a satellite-based Earth observation system that provides multispectral imagery at a 30×30 m resolution (Vermote et al., 2016). Specifically, we used a Landsat 8 scene captured on August 26, 2022 (in the middle of our study period), with NDVI computed from Band 5 (*NIR*) and Band 4 (*Red*). In contrast, Lantmäteriet Orthophoto was derived from aerial imagery at a 0.4×0.4 m resolution taken in 2022, with NDVI computed from Band 4 (*NIR*) and Band 1 (*Red*) (Fig. S1c). This dataset was then resampled to a 2×2 m resolution for evaluating the effect of different spatial resolutions in the OPLS analysis.

■ Site index by site factors (sis)

This index represents the inherent capacity of a site to support tree growth and biomass production. It was estimated using a combination of site properties, including climate, ground vegetation, location, and soil characteristics; hence the name site index by site factors (sis) (Hägglund and Lundmark, 1977). A key advantage of this index is that it can be assessed when the dominant tree height cannot be measured (e.g., after clearcutting or thinning from above) or when tree age is unknown. This flexibility has made it a standard indicator of forest productivity in the Swedish National Forest Inventory (NFI) since 2003. This index is species specific and is expressed as the expected height at a reference age of 100 years in even aged stands. In our study, sis values ranged between 8 and 23 m for the dominant tree species in a plot, either spruce or pine (0 m is assigned to clearcuts). This variable was collected in the Krycklan forest survey 2019/2020.

■ Stem density (stm)

Stem density (stm) represents the number of tree stems per hectare with a DBH greater than 4 cm. It is typically expressed as stems per hectare (stems/ha) and provides a quantitative measure of tree abundance within a given area. In our 78 study plots, values generally ranged from approximately 380 to 2,900 stems/ha, except for clearcuts, where stem density was 0. This variable was collected in the Krycklan forest survey 2019/2020.

S1.3.2 Species composition

■ Volume of birch species (bir)

This variable represents the total volume of birch trees, including the volume of the stem, top, and bark, within a plot. It is measured in cubic meters per hectare (m³/ha). Across our 78 study plots, the volume of birch varied from 0 to 77 m³/ha. This variable was collected in the Krycklan forest survey 2019/2020.

■ SLU birch map (bir-slu)

This variable represents the stem volume of birch trees, measured in cubic meters per hectare (m³/ha). Values refer to year 2010 and were extracted from a 25×25 m grid. Within our 78 study plots, bir-slu values ranged between 0 and 76 m³/ha.

■ Volume of pine species (pi)

This variable represents the total volume of pine trees, including the volume of stem, top, and bark, within a plot. It is measured in cubic meters per hectare (m³/ha). Across our 78 study plots, the volume of pine ranged between 0 and 316 m³/ha. This variable was collected in the Krycklan forest survey 2019/2020.

■ SLU pine map (pi-slu)

This variable represents the stem volume of pine trees, measured in cubic meters per hectare (m³/ha). Values refer to year 2010 and were extracted from a 25×25 m grid. Within our 78 study plots, pi-slu values ranged between 0 and 181 m³/ha.

■ Volume of spruce species (spr)

This variable represents the total volume of spruce trees, including the volume of stem, top, and bark, within a plot. It is measured in cubic meters per hectare (m³/ha). Across our 78 study plots, the volume of spruce varied from 0 to 667 m³/ha. This variable was collected in the Krycklan forest survey 2019/2020.

■ SLU spruce map (spr-slu)

This variable represents the stem volume of spruce trees, measured in cubic meters per hectare (m³/ha). Values refer to year 2010 and were extracted from a 25×25 m grid. Within our 78 study plots, spr-slu values ranged between 0 and 326 m³/ha.

S1.3.3 Forest structure

■ Canopy openness (co)

This variable quantifies the proportion (measured in percentage) of the sky visible through the forest canopy, serving as an indicator of forest structure and light availability to understory vegetation. Higher values denote more open canopies with greater sunlight penetration, while lower values indicate denser canopies with increased shading. To assess canopy openness, hemispherical photographs were taken at each datalogger location during the field campaign between June 27 and July 4, 2022. These photographs were processed and analyzed using two distinct methods:

Photosphere at eye height (about 150 cm above ground) with hemispheR Package (Chianucci and Macek, 2023):
 utilizing the Photosphere function on a smartphone, 360 degree spherical images were captured. These images were then processed with the hemispheR package in R, which offers an automated and reproducible approach for analyzing

hemispherical images to derive canopy structure metrics, including canopy openness (i.e., the proportion of sky pixels in a binarized image).

Lumix Camera with ImageJ Software: photographs were taken at 60 cm above ground using a Lumix digital camera
equipped with a fisheye lens. The images were subsequently analyzed using ImageJ, a widely-used image processing
program. With the macro "Hemispherical 2.0", images were converted to binary format to distinguish between sky
and canopy, allowing for the calculation of canopy openness.

Values for this variable usually ranged between about 6% and 56% in our 78 study plots, except for clearcuts, which were assigned a value of 100%.

■ Basal area weighted mean diameter (dgv)

This variable represents the mean DBH of trees within a plot, weighted by their contribution to the total basal area. It is calculated as follows:

$$dgv = \frac{\sum_{i=1}^{n} w_i d_i^3}{\sum_{i=1}^{n} w_i d_i^2},$$
(S8)

where n is the total number of sampled trees in the plot, w_i is the expansion factor representing how many trees the sampled tree i represents, and d_i is the DBH (in cm) for sampled tree i. This weighting gives greater influence to larger trees, reflecting their proportional impact on stand structure. Across our 78 study plots, dgv values ranged from approximately 8 cm to 36 cm, with a value of 0 assigned to clearcuts. This variable was collected in the Krycklan forest survey 2019/2020.

■ Basal area weighted mean height (hgv)

This variable represents the mean height of trees within a plot, weighted by their contribution to the total basal area. It is calculated as follows:

$$hgv = \frac{\sum_{i=1}^{n} w_{i}g_{i}h_{i}}{\sum_{i=1}^{n} w_{i}g_{i}},$$
(S9)

where n is the number of sampled trees, w_i is the expansion factor representing how many trees each sampled tree i stands for, g_i is the basal area at breast height of sampled tree i, and h_i is the height of sampled tree i. This calculation gives more weight to taller trees with larger basal areas. Across our 80 study plots, hgv values ranged between about 6 and 26 m, with a value of 0 assigned to clearcut areas. This variable was collected in the Krycklan forest survey 2019/2020.

■ SLU basal area weighted mean height map (hgv-slu)

This variable represents the mean tree height weighted by the basal area, where each tree's contribution to the average is proportional to its basal area, thus assigning greater influence to larger, structurally dominant trees within the stand. Values, expressed in meters (m), refer to year 2010 and were extracted from a 25×25 m grid. Within our 78 study plots, hgv-slu values ranged between 0 and 22 m.

■ Volume of all tree species (vol)

This variable represents the total volume of all tree species combined, including the stem, top, and bark, within a plot. It is measured in cubic meters per hectare (m³/ha). The total volume of all species across our 78 study plots ranged between 21 and 667 m³/ha, except for clearcut areas that were assigned a value of 0. This variable was collected in the Krycklan forest survey 2019/2020.

■ <u>SLU forest volume map (vol-slu)</u>

This variable represents the total stem volume of all tree species, measured in cubic meters per hectare (m³/ha). Values refer to year 2010 and were extracted from a 25×25 m grid. Within our 78 study plots, vol-slu values ranged between 0 and 365 m³/ha.

S1.4 Land use/land cover (LULC)

Land map (lm)

This vector map (Fig. S1d) illustrates the main LULC types by combining physical land cover (forest, peatland, open land, water bodies, and urban surfaces) with human-defined land use (arable land, clearcut, transportation network). Rather than treating land cover and land use separately, the map integrates both aspects to provide a comprehensive representation of the landscape. The classification is based on data from two sources: the Lantmäteriet Property map at the scale of 1:10,000 (Lantmäteriet, 2023) and clearcut records in vector format from Skogsstyrelsen (Skogsstyrelsen, 2024). Three LULC types were identified at the locations of the dataloggers used in this study (Fig. S1d):

- Clearcut (lm-cut): areas where clearcutting occurred between September 1, 2001, and July 4, 2022 (just before the beginning of soil moisture recording); no new clearcuts occurred during our study period (July 5 October 4, 2022).
- Forest (lm-for): includes coniferous and mixed forest.
- Peatland (lm-ptl): originally, peatland and wet peatland were distinct classes, characterized by different degrees of
 accessibility; however, since no logger was placed in wet peatland, these two classes are combined in Fig. S1d for
 simplicity.

■ Land survey (ls)

This variable represents the LULC classification based on field surveys conducted during the installation of soil moisture loggers in June/July 2022 and the subsequent data collection in October 2022. The categories are similar to those in the land map (lm) but were determined directly in the field, providing an on-site assessment of LULC conditions:

- Clearcut (ls-cut): areas where logging had recently occurred, characterized by open ground with residual vegetation and logging debris.
- Forest (ls-for): coniferous and mixed forest stands with tree cover and understory vegetation.
- Peatland (ls-ptl): wetland areas with peat accumulation, identified in the field based on vegetation and soil characteristics.

S2. Temporal predictors (refer to Table 2 in the main manuscript)

These variables were used to predict temporal variability in soil moisture.

S2.1 Air temperature

■ 2 m dewpoint temperature (d2m)

ERA5-Land (Muñoz-Sabater, 2019). This parameter represents the temperature to which the air, at 2 m above the Earth's surface, would have to be cooled for saturation to occur. The original unit was kelvin (K), but it was converted to degrees Celsius (°C) by subtracting 273.15.

■ Skin temperature (skt)

ERA5-Land (Muñoz-Sabater, 2019). This parameter represents the temperature of the Earth's surface. The skin temperature is the theoretical temperature required to satisfy the surface energy balance. It represents the temperature of the uppermost surface layer, which has no heat capacity and can therefore respond instantaneously to changes in surface fluxes. The original unit was kelvin (K), but it was converted to degrees Celsius (°C) by subtracting 273.15.

■ 2 m temperature (t2m)

ERA5-Land (Muñoz-Sabater, 2019). This parameter represents the temperature of air at 2 m above the surface of land, sea, or in-land waters. The original unit was kelvin (K), but it was converted to degrees Celsius (°C) by subtracting 273.15.

■ Air temperature (ta)

Automatic weather stations (Svartberget Research Station, 2022b, c). This parameter represents the temperature of air at 1.7 m above ground. It was measured at two locations using a PT100/3 sensor. A vented radiation shield protects the sensor from direct solar radiation. The temperature was recorded as a daily average based on 1 min scans. The overall daily average was then calculated between the two stations (Åheden and Hygget in Fig. 1). The measurement unit is degrees Celsius (°C).

Air temperature level 1

ICOS tower (Peichl et al., 2024). This parameter represents the temperature of air at 42 m above ground. It was measured using a Scientific Campbell 105E sensor based on 10 sec scans. The original dataset had a 30 min temporal resolution, from which we calculated daily averages. The measurement unit is degrees Celsius (°C).

Air temperature level 2

ICOS tower (Peichl et al., 2024). This parameter represents the temperature of air at 30 m above ground. It was measured using a Scientific Campbell 105E sensor based on 10 sec scans. The original dataset had a 30 min temporal resolution, from which we calculated daily averages. The measurement unit is degrees Celsius (°C).

Air temperature level 3

ICOS tower (Peichl et al., 2024). This parameter represents the temperature of air at 20 m above ground. It was measured using a Scientific Campbell 105E sensor based on 10 sec scans. The original dataset had a 30 min temporal resolution, from which we calculated daily averages. The measurement unit is degrees Celsius (°C).

■ Air temperature level 4

ICOS tower (Peichl et al., 2024). This parameter represents the temperature of air at 10 m above ground. It was measured using a Scientific Campbell 105E sensor based on 10 sec scans. The original dataset had a 30 min temporal resolution, from which we calculated daily averages. The measurement unit is degrees Celsius (°C).

S2.2 Air water

■ Air relative humidity (rh)

ICOS tower (Peichl et al., 2024). This parameter represents the ratio of the actual amount of water vapor in the air to the maximum amount that the air could hold at a given temperature, expressed as a percentage (%). It indicates how close the air is to being saturated with moisture. It was measured at 32.5 m above ground using a Rotronic HC2(A)-S sensor based on 5 sec scans. The original dataset had a 30 min temporal resolution, from which we calculated daily averages.

Skin reservoir content (src)

ERA5-Land (Muñoz-Sabater, 2019). This parameter represents the amount of water in the vegetation canopy and/or in a thin layer on the soil. It includes rain intercepted by foliage as well as water from dew. The maximum amount of "skin reservoir content" a grid box can hold depends on the type of vegetation, and may be zero. Water exits the "skin reservoir" through evaporation. The original unit was meters of water equivalent, but it was converted to millimeters (mm).

S2.3 Evaporation

■ <u>Total evaporation (e)</u>

ERA5-Land (Muñoz-Sabater, 2019). This parameter represents the accumulated amount of water that has evaporated from the Earth's surface, including a simplified representation of transpiration (from vegetation), into vapor in the air above. By convention, downward fluxes are positive; thus, negative values indicate evaporation and positive values indicate condensation. The original unit was meters of water equivalent, but it was converted to millimeters (mm).

■ Evaporation from bare soil (ebs)

ERA5-Land (Muñoz-Sabater, 2019). This parameter represents the accumulated amount of evaporation from bare soil at the top of the land surface. The original unit was meters of water equivalent, but it was converted to millimeters (mm).

■ Potential evaporation (ep)

ERA5-Land (Muñoz-Sabater, 2019). This parameter indicates the extent to which near-surface atmospheric conditions are conducive to evaporation. It is generally defined as the accumulated amount of evaporation that would occur from a pure water surface at the temperature of the lowest atmospheric layer under current atmospheric conditions. It provides a measure of the maximum possible evaporation. The original unit was meters of water equivalent, but it was converted to millimeters (mm).

Evaporation from the top of the canopy (etc)

ERA5-Land (Muñoz-Sabater, 2019). This parameter represents the accumulated amount of evaporation from the canopy interception reservoir. The original unit was meters of water equivalent, but it was converted to millimeters (mm).

■ Evaporation from vegetation transpiration (evt)

ERA5-Land (Muñoz-Sabater, 2019). This parameter represents the accumulated amount of evaporation from vegetation transpiration. It is equivalent to root extraction (i.e., the amount of water extracted from different soil layers). The original unit was meters of water equivalent, but it was converted to millimeters (mm).

S2.4 Heat

■ Soil heat flux level 1 (sh1)

ICOS tower (Peichl et al., 2024). This parameter represents the amount of thermal energy transferred between the soil and the atmosphere per unit area and time. The soil heat flux is positive when the soil receives energy (warms) and negative when the soil loses energy (cools). It was measured at the surface using a Hukseflux HFP01SC sensor based on 10 sec scans. The original dataset had a 30 min temporal resolution, from which we calculated daily averages. The measurement unit is joule per square meter per second (J m⁻² s⁻¹), that is watt per square meter (W m⁻²).

■ Soil heat flux level 2 (sh2)

ICOS tower (Peichl et al., 2024). This parameter represents the amount of thermal energy that moves through an area of soil in a unit of time. By convention, vertical fluxes are positive when directed downward and negative when directed upward. It was measured at 5 cm below surface using a Hukseflux HFP01SC sensor based on 10 sec scans. The original dataset had a 30 min temporal resolution, from which we calculated daily averages. The measurement unit is joule per square meter per second (J m⁻² s⁻¹), that is watt per square meter (W m⁻²).

■ Surface sensible heat flux (shf)

ERA5-Land (Muñoz-Sabater, 2019). This parameter represents the accumulated amount of heat transferred between the Earth's surface and the atmosphere due to turbulent air motion, excluding heat transfer from condensation or evaporation. The magnitude of sensible heat flux is governed by the temperature difference between the surface and the overlying atmosphere, wind speed, and surface roughness. For instance, cold air overlying a warm surface generates a sensible heat flux from the land or ocean into the atmosphere. By convention, vertical fluxes are positive when directed downward. The units are joules per square meter (J m⁻²).

S2.5 Precipitation

■ Total precipitation (p)

ERA5-Land (Muñoz-Sabater, 2019). This parameter represents the accumulated liquid and frozen water, including rain and snow, that falls to the Earth's surface. It is the sum of large-scale precipitation (produced by large-scale weather patterns, such as troughs and cold fronts) and convective precipitation (resulting from convection, which occurs when warmer, less dense air at lower atmospheric levels rises). This parameter does not account for fog, dew, and precipitation that evaporates in the atmosphere before reaching the surface. The original unit of precipitation was depth in meters, but it was converted to millimeters (mm). This depth represents the amount of water evenly distributed over the grid box.

■ Total precipitation (pr)

Automatic weather stations (Svartberget Research Station, 2022b, c). This parameter represents the accumulated amount of precipitation measured using an SMHI rain gauge located 1.5 m above ground. Precipitation is recorded as a daily total in millimeters (mm). The daily totals are then averaged between the two stations (Åheden and Hygget in Fig. 1).

S2.6 Pressure

Air pressure (pa)

Automatic weather stations (Svartberget Research Station, 2022a). The daily average of air pressure was measured at the Stortjärn station (Fig. 1) using a VAISALA PTB110 sensor based on a 5 sec sampling interval. The original unit was pascal (Pa), but it was converted to hectopascal (hPa).

Surface pressure (sp)

ERA5-Land (Muñoz-Sabater, 2019). This parameter represents the pressure (force per unit area) exerted by the atmosphere on the surface of land, sea, and inland water. It measures the weight of all the air in a column vertically above a fixed point on the Earth's surface. The original unit was pascal (Pa), but it was converted to hectopascal (hPa).

■ Vapor pressure (vp)

Automatic weather stations (Svartberget Research Station, 2022b, c). This parameter represents the pressure of water vapor at 1.7 m above ground. The daily average was measured at two locations using two different sensors (Hygrometer Humiclip based on 1 min scans and Rotronic MP103A-T4-W4W based on 5 sec scans). The overall daily average was then calculated between the two stations (Åheden and Hygget in Fig. 1). The measurement unit is hectopascal (hPa).

■ Vapor pressure deficit (vpd)

ICOS tower (Peichl et al., 2024). This parameter represents the difference between the saturated vapor pressure and the actual vapor pressure. A higher vpd value indicates drier air, suggesting greater potential for evaporation or transpiration. It was measured at 32.5 m above ground using a Rotronic HC2(A)-S sensor based on 5 sec scans. The original dataset had a 30 min temporal resolution, from which we calculated daily averages. The measurement unit is hectopascal (hPa).

S2.7 Radiation

Forecast albedo (fal)

ERA5-Land (Muñoz-Sabater, 2019). This parameter measures the reflectivity of the Earth's surface, expressed as the fraction of solar (shortwave) radiation reflected across the solar spectrum, including both direct and diffuse radiation. Values are between 0 and 1. Snow and ice typically have high reflectivity, with albedo values of 0.8 or higher, land surfaces have intermediate values, ranging from about 0.1 to 0.4, while the ocean has low reflectivity, with albedo values of 0.1 or less. Solar radiation (shortwave radiation) is partially reflected back to space by clouds and atmospheric particles (aerosols), while some is absorbed. The remainder reaches the Earth's surface, where a portion is reflected back. The amount reflected depends on the surface's albedo.

Long wave incoming radiation (lwi)

ICOS tower (Peichl et al., 2024). This parameter represents the infrared radiation emitted by the atmosphere (greenhouse gases, clouds, and other atmospheric constituents) and directed toward the Earth's surface. This radiation typically has wavelengths ranging from about 4 to 100 micrometers (μ m). It was measured at 50 m above ground using a pyranometer (SW - ISO 9060:1990 secondary standard, Kipp&Zonen, CMP21) based on 5 sec scans. The original dataset had a 30 min temporal resolution, from which we calculated daily averages. The measurement unit is joule per square meter per second (J m⁻² s⁻¹), that is watt per square meter (W m⁻²).

Long wave outgoing radiation (lwo)

ICOS tower (Peichl et al., 2024). This parameter represents the infrared radiation emitted from the Earth's surface back into the atmosphere, which mostly depends on surface temperature and emissivity. This radiation typically has wavelengths ranging from about 4 to 100 micrometers (μm). It was measured at 50 m above ground using a pyranometer (SW - ISO 9060:1990 secondary standard, Kipp&Zonen, CMP21) based on 5 sec scans. The original dataset had a 30 min temporal resolution, from which we calculated daily averages. The measurement unit is joule per square meter per second (J m⁻² s⁻¹), that is watt per square meter (W m⁻²).

Surface net solar radiation (nsr)

ERA5-Land (Muñoz-Sabater, 2019). This parameter represents the accumulated amount of solar radiation (also known as shortwave radiation) that reaches a horizontal plane at the Earth's surface (both direct and diffuse), minus the portion reflected by the surface, which is determined by the albedo. Solar radiation is partially reflected back to space by clouds and atmospheric particles (aerosols), while some is absorbed. The remainder reaches the Earth's surface, where a portion is reflected. By convention, vertical fluxes are positive when directed downward. The units are joules per square meter (J m⁻²).

Surface net thermal radiation (ntr)

ERA5-Land (Muñoz-Sabater, 2019). This parameter represents the accumulated net thermal radiation (also known as longwave or terrestrial radiation) at the Earth's surface, calculated as the difference between downward and upward thermal radiation passing through a horizontal plane. The atmosphere and clouds emit thermal radiation in all directions, with a portion reaching the surface as downward thermal radiation. Upward thermal radiation at the surface includes radiation emitted by the surface and the fraction of downward thermal radiation reflected upward by the surface. By convention, vertical fluxes are positive when directed downward. The units are joules per square meter (J m⁻²).

Short wave incoming radiation (swi)

ICOS tower (Peichl et al., 2024). This parameter represents the solar radiation received by the Earth's atmosphere and surface. It primarily consists of visible light and ultraviolet radiation, with wavelengths generally ranging from 0.1 to 4 micrometers (µm). It was measured at 50 m above ground using a pyranometer (SW - ISO 9060:1990 secondary standard, Kipp&Zonen, CMP21) based on 5 sec scans. The original dataset had a 30 min temporal resolution, from which we calculated daily averages. The measurement unit is joule per square meter per second (J m⁻² s⁻¹), that is watt per square meter (W m⁻²).

Short wave outgoing radiation (swo)

ICOS tower (Peichl et al., 2024). This parameter represents the portion of the incoming solar radiation that is reflected back into the atmosphere, which mostly depends on surface albedo (reflectivity). It primarily consists of visible light and ultraviolet radiation, with wavelengths generally ranging from 0.1 to 4 micrometers (μm). It was measured at 50 m above ground using a pyranometer (SW - ISO 9060:1990 secondary standard, Kipp&Zonen, CMP21) based on 5 sec scans. The original dataset had a 30 min temporal resolution, from which we calculated daily averages. The measurement unit is joule per square meter per second (J m⁻² s⁻¹), that is watt per square meter (W m⁻²).

Surface thermal radiation downwards (trd)

ERA5-Land (Muñoz-Sabater, 2019). This parameter represents the accumulated amount of thermal radiation (also known as longwave or terrestrial radiation) emitted by the atmosphere and clouds that reaches a horizontal plane at the Earth's surface. By convention, vertical fluxes are positive when directed downward. The units are joules per square meter (J m⁻²).

S2.8 Runoff

■ Runoff (ro)

ERA5-Land (Muñoz-Sabater, 2019). This parameter represents the accumulated amount of water from rainfall, snowmelt or soil storage that drains away, either over the surface (surface runoff) or under the ground (sub-surface runoff). The original unit of runoff was depth in meters, but it was converted to millimeters (mm). This depth represents the amount of water evenly distributed over the grid box.

■ Surface runoff (sr)

ERA5-Land (Muñoz-Sabater, 2019). This parameter represents the accumulated amount of water that flows over the Earth's surface when it is not absorbed by the soil. Surface runoff usually occurs due to rainfall or melting snow exceeding the infiltration capacity of the soil. The original unit of surface runoff was depth in meters, but it was converted to millimeters (mm). This depth represents the amount of water evenly distributed over the grid box.

■ Sub-surface runoff (ssr)

ERA5-Land (Muñoz-Sabater, 2019). This parameter represents the accumulated amount of water that drains beneath the surface through soil layers and underground pathways. Sub-surface runoff usually occurs when water infiltrates the soil but continues to move laterally. The original unit of sub-surface runoff was depth in meters, but it was converted to millimeters (mm). This depth represents the amount of water evenly distributed over the grid box.

S2.9 Soil temperature

■ Soil temperature level 1 (st1)

ERA5-Land (Muñoz-Sabater, 2019). This parameter represents the temperature of the soil in the middle of layer 1 (0–7 cm below surface). The original unit was kelvin (K), but it was converted to degrees Celsius (°C) by subtracting 273.15.

■ Soil temperature level 2 (st2)

ERA5-Land (Muñoz-Sabater, 2019). This parameter represents the temperature of the soil in the middle of layer 2 (7–28 cm below surface). The original unit was kelvin (K), but it was converted to degrees Celsius (°C) by subtracting 273.15.

■ Soil temperature level 3 (st3)

ERA5-Land (Muñoz-Sabater, 2019). This parameter represents the temperature of the soil in the middle of layer 3 (28–100 cm below surface). The original unit was kelvin (K), but it was converted to degrees Celsius (°C) by subtracting 273.15.

■ Soil temperature level 4 (st4)

ERA5-Land (Muñoz-Sabater, 2019). This parameter represents the temperature of the soil in the middle of layer 4 (100–289 cm below surface). The original unit was kelvin (K), but it was converted to degrees Celsius (°C) by subtracting 273.15.

■ Soil temperature level 1 (ts1)

Automatic weather stations (Svartberget Research Station, 2022b). This parameter represents the temperature of the soil at a depth of 10 cm below surface. The daily average was measured at the Åheden station (Fig. 1) using a PT100 sensor based on 1 min scans. The measurement unit is degrees Celsius (°C).

■ Soil temperature level 2 (ts2)

Automatic weather stations (Svartberget Research Station, 2022b, c). This parameter represents the temperature of the soil at a depth of 20 cm below surface. The daily average was measured at two locations using a PT100 sensor based on 1 min scans. The overall daily average was then calculated between the two stations (Åheden and Hygget in Fig. 1). The measurement unit is degrees Celsius (°C).

■ Soil temperature level 3 (ts3)

ICOS tower (Peichl et al., 2024). This parameter represents the temperature of the soil at a depth of 30 cm below surface. It was measured using a Scientific Campbell 105E sensor based on 10 sec scans. The original dataset had a 30 min temporal resolution, from which we calculated daily averages. The measurement unit is degrees Celsius (°C).

■ Soil temperature level 4 (ts4)

ICOS tower (Peichl et al., 2024). This parameter represents the temperature of the soil at a depth of 50 cm below surface. It was measured using a Scientific Campbell 105E sensor based on 10 sec scans. The original dataset had a 30 min temporal resolution, from which we calculated daily averages. The measurement unit is degrees Celsius (°C).

S2.10 Soil water

Soil water content level 1 (sm1)

ICOS tower (Peichl et al., 2024). This parameter represents the volumetric water content in the soil at a depth of 2.5 cm below surface. It was measured using a Delta-T ML ThetaProbe sensor based on 10 sec scans. The original dataset had a 30 min temporal resolution, from which we calculated daily averages. The measurement unit is percentage (%).

Soil water content level 2 (sm2)

ICOS tower (Peichl et al., 2024). This parameter represents the volumetric water content in the soil at a depth of 5 cm below surface. It was measured using a Delta-T ML ThetaProbe sensor based on 10 sec scans. The original dataset had a 30 min temporal resolution, from which we calculated daily averages. The measurement unit is percentage (%).

Soil water content level 3 (sm3)

ICOS tower (Peichl et al., 2024). This parameter represents the volumetric water content in the soil at a depth of 10 cm below surface. It was measured using a Delta-T ML ThetaProbe sensor based on 10 sec scans. The original dataset had a 30 min temporal resolution, from which we calculated daily averages. The measurement unit is percentage (%).

Soil water content level 4 (sm4)

ICOS tower (Peichl et al., 2024). This parameter represents the volumetric water content in the soil at a depth of 30 cm below surface. It was measured using a Delta-T ML ThetaProbe sensor based on 10 sec scans. The original dataset had a 30 min temporal resolution, from which we calculated daily averages. The measurement unit is percentage (%).

■ Volumetric soil water level 1 (sw1)

ERA5-Land (Muñoz-Sabater, 2019). This parameter represents the volume of water in soil layer 1 (0–7 cm below surface). The volumetric soil water is associated with the soil texture, soil depth, and the underlying groundwater level. The original unit was m³/m³, but it was converted to percentage (%).

■ Volumetric soil water level 2 (sw2)

ERA5-Land (Muñoz-Sabater, 2019). This parameter represents the volume of water in soil layer 2 (7–28 cm below surface). The volumetric soil water is associated with the soil texture, soil depth, and the underlying groundwater level. The original unit was m³/m³, but it was converted to percentage (%).

■ Volumetric soil water level 3 (sw3)

ERA5-Land (Muñoz-Sabater, 2019). This parameter represents the volume of water in soil layer 3 (28–100 cm below surface). The volumetric soil water is associated with the soil texture, soil depth, and the underlying groundwater level. The original unit was m³/m³, but it was converted to percentage (%).

■ Volumetric soil water level 4 (sw4)

ERA5-Land (Muñoz-Sabater, 2019). This parameter represents the volume of water in soil layer 4 (100–289 cm below surface). The volumetric soil water is associated with the soil texture, soil depth, and the underlying groundwater level. The original unit was m³/m³, but it was converted to percentage (%).

S2.11 Vegetation

■ Leaf area index, high vegetation

ERA5-Land (Muñoz-Sabater, 2019). This parameter is defined as one-half of the total green leaf area per unit of horizontal ground surface for vegetation classified as 'high'. High vegetation includes evergreen trees, deciduous trees, mixed forests/woodlands, and interrupted forests. It has a value of 0 over bare ground or where there are no leaves. The unit is m²/m².

■ Photosynthetic photon flux density below canopy incoming (pbc)

ICOS tower (Peichl et al., 2024). This parameter represents the amount of photosynthetically active radiation (PAR) that penetrates through the canopy and reaches the lower layers beneath it. It provides insights into light availability for understory plants and the efficiency of canopy light interception. It was measured at 1.15 m above ground using a LI-COR LI190R quantum sensor based on 5 sec scans. The original dataset had a 30 min temporal resolution, from which we calculated daily averages. The measurement unit is micromoles of photons per square meter per second (µmolPhotons/m²/s).

■ Photosynthetic photon flux density diffuse (pd)

ICOS tower (Peichl et al., 2024). This parameter represents the amount of photosynthetically active radiation (PAR) that has been scattered by atmospheric particles, clouds, or other elements, reaching a surface uniformly from all directions. Diffuse light is critical for plant photosynthesis as it penetrates deeper into plant canopies compared to direct light. It was measured at 50 m above ground using a LI-COR LI190R quantum sensor based on 5 sec scans. The original dataset had a 30 min temporal resolution, from which we calculated daily averages. The measurement unit is micromoles of photons per square meter per second (μmolPhotons/m²/s).

■ Photosynthetic photon flux density incoming (pi)

ICOS tower (Peichl et al., 2024). This parameter represents the total amount of photosynthetically active radiation (PAR) arriving at a horizontal surface, combining both direct sunlight and diffuse light. It was measured at 50 m above ground using a LI-COR LI190R quantum sensor based on 5 sec scans. The original dataset had a 30 min temporal resolution, from which we calculated daily averages. The measurement unit is micromoles of photons per square meter per second (umolPhotons/m²/s).

■ Photosynthetic photon flux density outgoing (po)

ICOS tower (Peichl et al., 2024). This parameter represents the amount of photosynthetically active radiation (PAR) that is reflected or scattered away from a surface, such as a canopy or the ground. It helps assess the albedo effect of vegetation or soil and its impact on energy balance and light use efficiency. This parameter was measured at 50 m above ground using a LI-COR LI190R quantum sensor based on 5 sec scans. The original dataset had a 30 min temporal resolution, from which we calculated daily averages. The measurement unit is micromoles of photons per square meter per second (μmolPhotons/m²/s).

S2.12 Wind

■ 10 m u-component of wind (u10)

ERA5-Land (Muñoz-Sabater, 2019). This parameter represents the eastward component of the 10 m wind. It is the horizontal speed of air moving towards the east, at a height of 10 m above the surface of the Earth, in meters per second (m/s).

■ 10 m v-component of wind (v10)

ERA5-Land (Muñoz-Sabater, 2019). This parameter represents the northward component of the 10 m wind. It is the horizontal speed of air moving towards the north, at a height of 10 m above the surface of the Earth, in meters per second (m/s).

■ Wind direction respect to geographic north (wd)

ICOS tower (Peichl et al., 2024). This parameter represents the direction from which the wind originates, expressed in degrees relative to geographic north (degree N). It was measured at 34.5 m above ground using an anemometer with high-frequency scans (0.05 seconds, 20 Hz) to capture rapid variations in wind directions. The original dataset had a 30 min temporal resolution, from which we calculated daily averages.

■ Wind speed (ws)

ICOS tower (Peichl et al., 2024). This parameter represents the rate at which air moves past the measurement point, expressed in meters per second (m/s). It was measured at 34.5 m above ground using an anemometer with high-frequency scans (0.05 seconds, 20 Hz) to track rapid wind velocity fluctuations. The original dataset had a 30 min temporal resolution, from which we calculated daily averages.

FIGURES AND TABLES

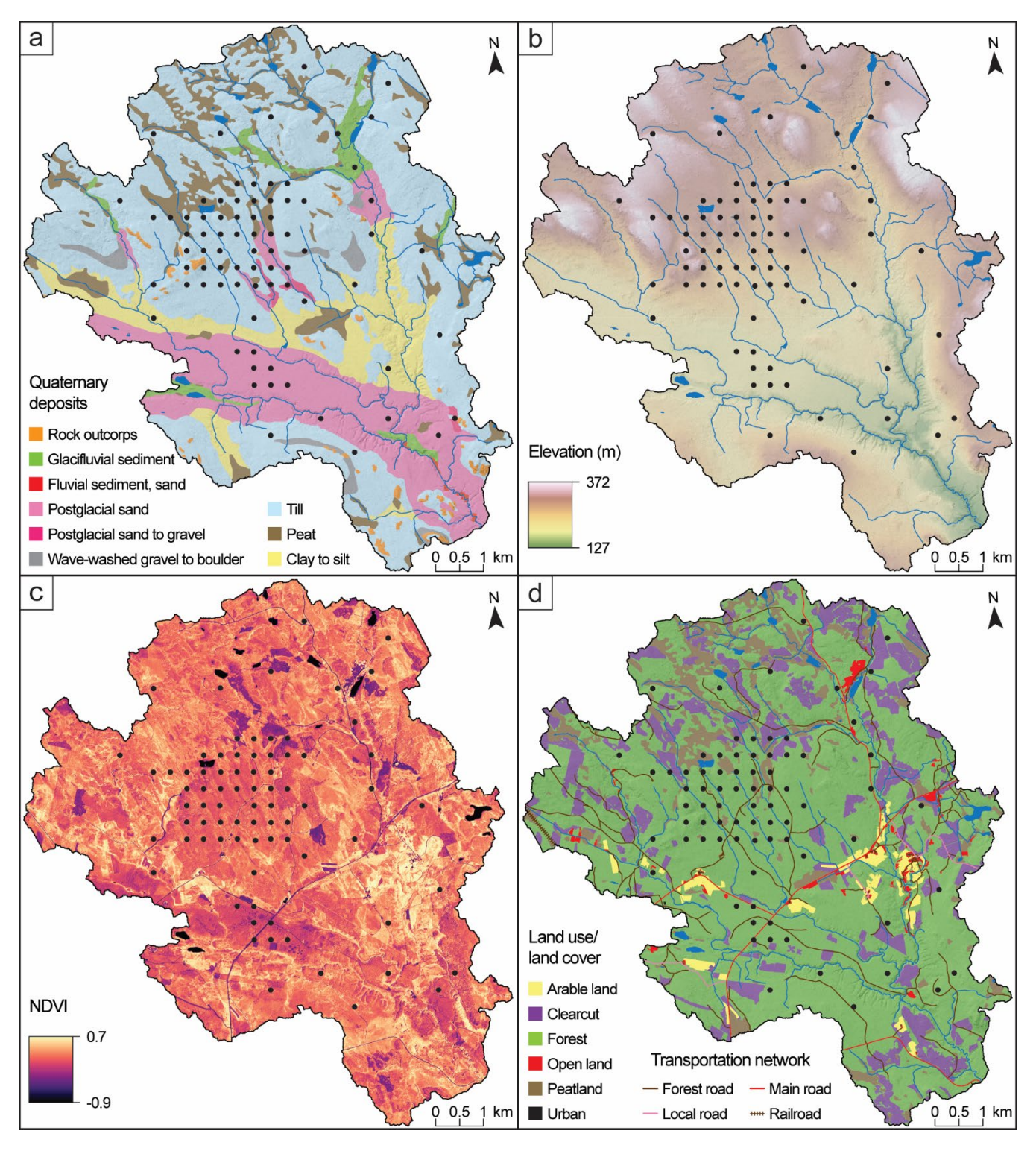


Figure S1. Environmental maps of the study area. (a) Quaternary deposits. (b) Elevation. (c) NDVI (Normalized Difference Vegetation Index). (d) Land use/land cover, including the transportation network. Maps in panels (a), (b), and (d) include a hillshade derived from the 0.5×0.5 m DEM for better visualization and display water bodies (lakes, rivers, and streams) in blue. In all panels, the locations of the 78 study plots, where soil moisture loggers were placed, are marked as black dots. Apparent discrepancies between panels (c) and (d) arise from differences in temporal coverage: clearcuts in panel (d) (shown in purple) represent areas logged between 2000 and 2022, whereas the NDVI in panel (c) was derived from aerial images taken in 2022. Older clearcut areas may have begun regenerating and thus exhibit different NDVI values compared to more recent clearcuts, leading to visual differences between the two panels.

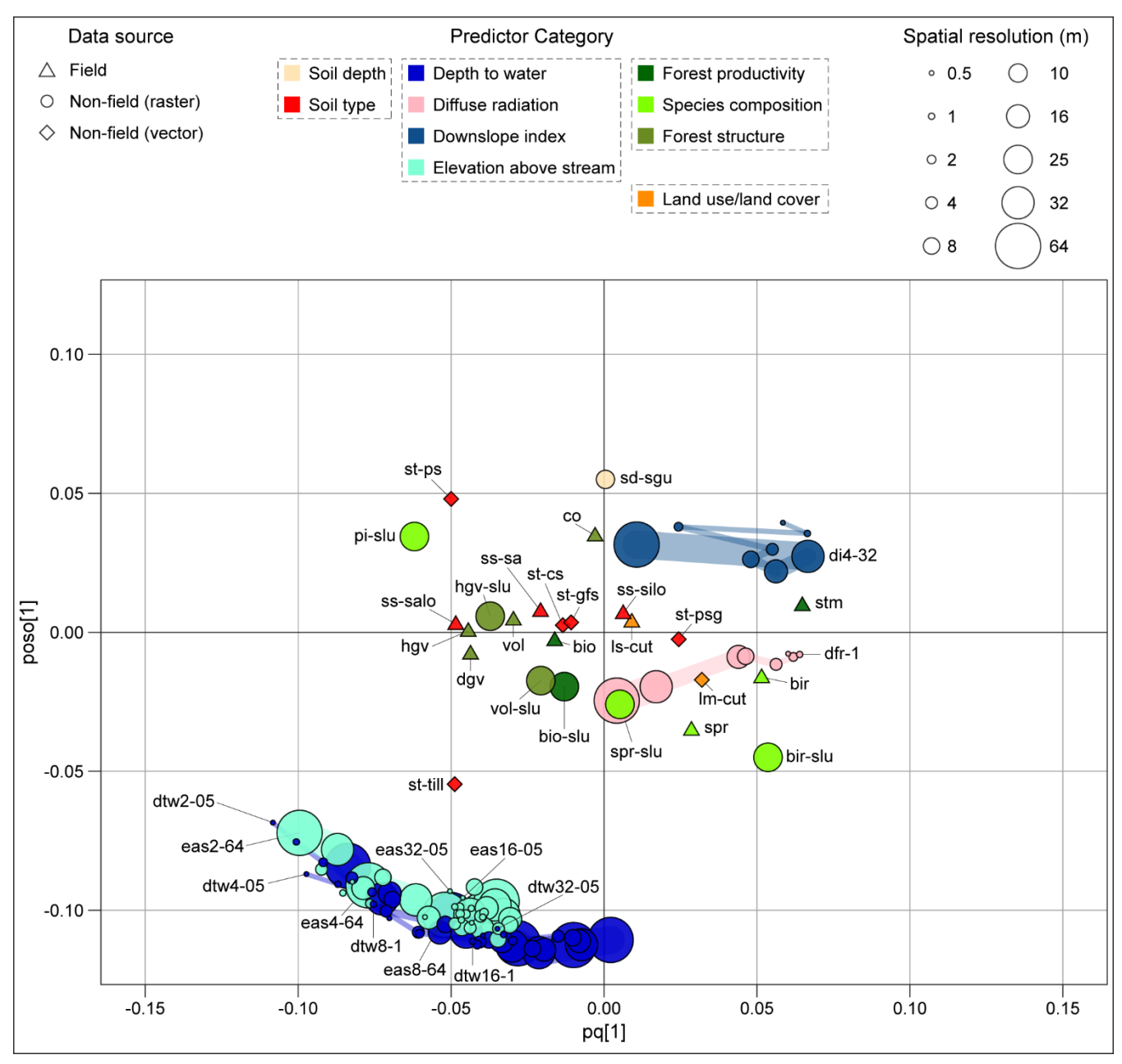


Figure S2. OPLS loading plot showing the relationship between a large array of "spatial" predictors, which vary spatially but remain constant over time, and the mean seasonal soil moisture (July 5 – October 4, 2022). Both the spatial predictors (X-variables) and the determinant (Y-variable) were gathered for 78 sites across the Krycklan catchment (Fig. 1 for the site locations). The spatial predictors, overall describing soil, topography, vegetation, and land use/land cover at each site (grey dotted boxes in the figure legend) were either directly measured in situ (symbolized by triangles) or estimated through remote sensing or modeling techniques (depicted as circles or rhombuses depending on the dataset format). These predictors were organized into 18 color-coded categories (see Table 1; here only 10 are shown) to enhance plot readability. Gridded (i.e., raster) predictors are characterized by a certain spatial resolution, represented by the size of the circles. To visualize the effects of spatial resolution, guides connect loadings of the same variable moving from high to low resolutions, with the variable name visible only in correspondence of the optimal resolution (refer to Table 1 for variable labels). High positive and negative loadings on the predictive axis (pq[1]) represent variables that are positively and negatively correlated with the response variable (Y), with stronger

correlation further away from the origin. The orthogonal axis (poso[1]) indicates how much of the variation for each variable was not correlated with the response variable (Y). This figure only shows the 26 least relevant predictors (VIP_{predictive} smaller than 1, without asterisk in Table 1) as well as the less-performing layers (i.e., non-optimal user-defined thresholds) of three topographic indices (i.e., depth to water, downslope index, and elevation above stream).

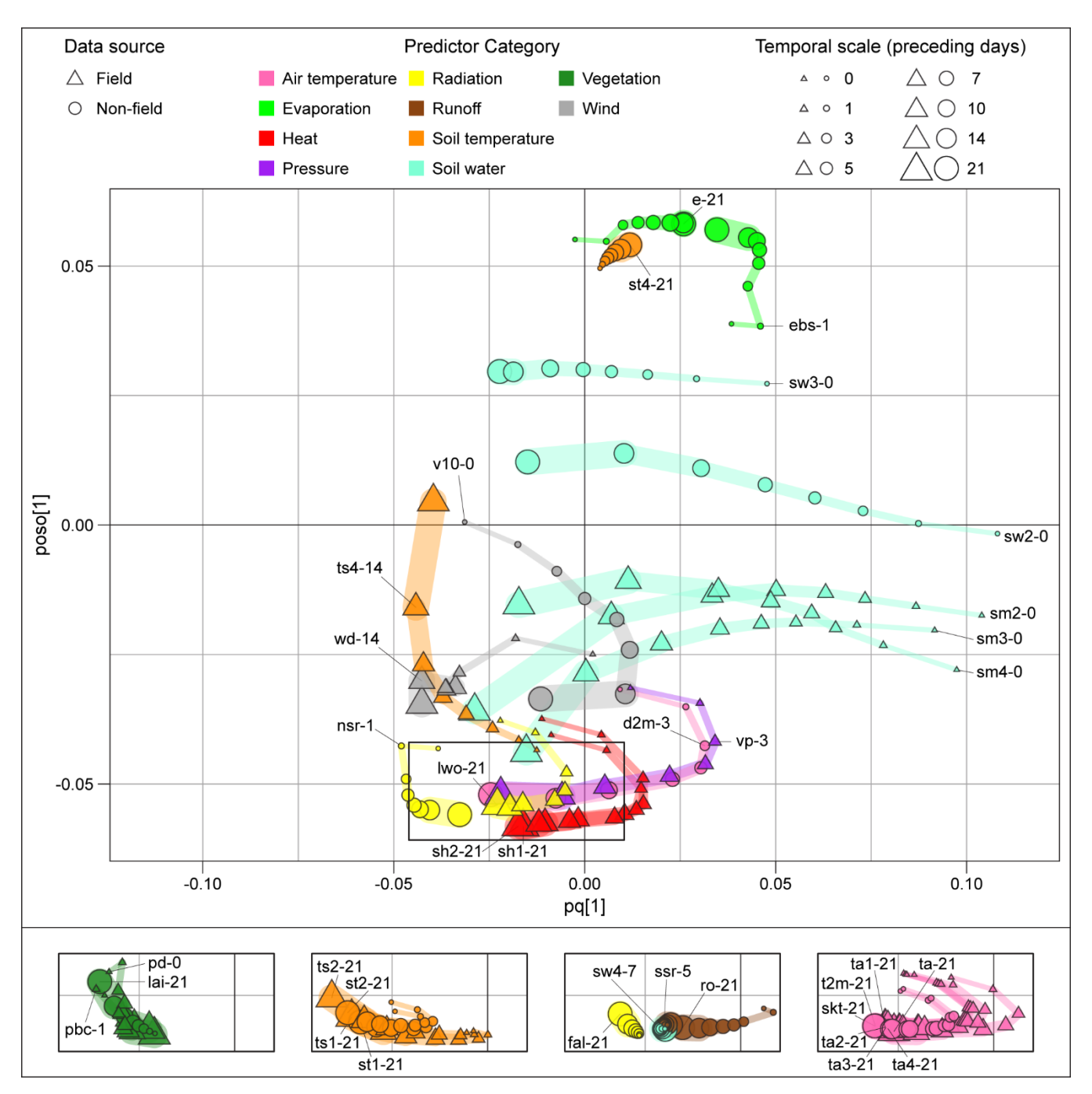


Figure S3. OPLS loading plot illustrating the relationship between a large array of "temporal" predictors, which do not vary spatially but change over time, and daily mean soil moisture (i.e., volumetric water content) averaged across 78 sites within the Krycklan catchment (refer to Fig. 1 for the site locations). Both the temporal predictors (X-variables) and the determinant (Y-variable) were aggregated at the daily temporal scale from July 5 to October 4, 2022. The temporal predictors were either directly measured at the ICOS tower or at weather stations within Krycklan (symbolized by triangles) or extracted from the ERA5-Land dataset (depicted as circles). These predictors were organized into 12 color-coded categories (see Table 2; here only 10 are shown) to enhance plot readability. All predictors are characterized by a certain temporal scale, represented by the size of the triangles or circles. To visualize the effects of temporal scale, guides connect

loadings of the same variable moving from high to low scales, with the variable name visible only in correspondence of the optimal scale (refer to Table 2 for variable labels). High positive and negative loadings on the predictive axis (pq[1]) represent variables that are positively and negatively correlated with the response variable (Y), with stronger correlation further away from the origin. The orthogonal axis (poso[1]) indicates how much of the variation for each variable was not correlated with the response variable (Y). This figure only shows the 35 least relevant predictors (VIP_{predictive} smaller than 1, without asterisk in Table 2). Because many variables that did not explain the temporal variability in soil moisture (including all air temperature predictors) clustered in the bottom-central part of the graphic, we quadruplicated that plot area (black rectangle box) to help visualize all overlapping loadings.

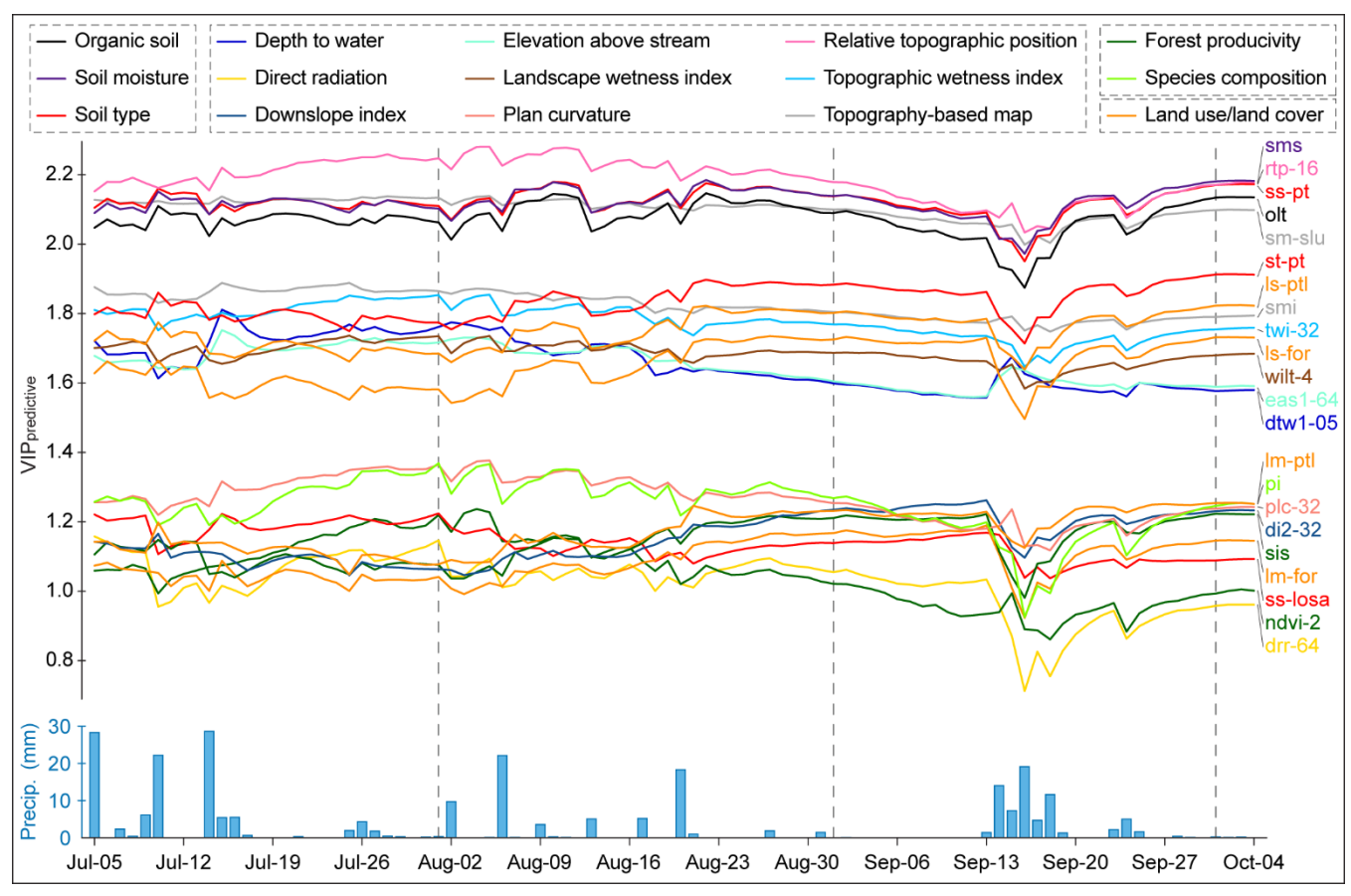


Figure S4. VIP_{predictive} values of 92 spatial OPLS models generated using mean daily soil moisture over the study season (July 5 – October 4, 2022) as the response variable (Y). The lower section of the figure displays the mean precipitation across Krycklan derived from weather stations (refer to Fig. 1 for their locations). The spatial predictors, overall describing soil, topography, vegetation, and land use/land cover at each site (grey dotted boxes in the figure legend), were organized into 18 color-coded categories (see Table 1; here only 15 are shown) to enhance plot readability. This graphic includes all 22 relevant predictors (VIP_{predictive} greater than 1) identified in Fig. 4. Color-coded labels on the right side of the figure are ordered according to their VIP_{predictive} on the last day of the study season (October 4, 2022).

Table S1. Results of the Mann-Kendall test for seasonal trends in soil moisture (July 5 – October 4, 2022) across 78 study plots. The table presents the p-value, Kendall's correlation coefficient (τ), Theil-Sen's slope, and the overall seasonal change in soil moisture (%). Study plots exhibiting significant positive trends (95% confidence interval) are highlighted in green (15), while those with significant negative trends are highlighted in purple (7). Refer to Fig. 2bc for details regarding location and daily time series plot associated with these trends.

Plot ID	p value	Kendall's τ	Theil-Sen's slope	Seasonal change (%)
19	0.66851	-0.06	-0.010	-1.0
39	0.81263	0.04	0.008	0.7
68	0.00268	-0.39	-0.049	-4.5
74	0.95169	-0.01	-0.001	-0.1
78	0.80788	0.02	0.006	0.5
82	0.93293	0.01	0.002	0.2
89	0.42147	0.08	0.011	1.0
128	0.94508	0.01	0.001	0.0
143	0.02439	0.25	0.025	2.3
144	0.35714	0.11	0.015	1.4
145	0.05644	0.24	0.015	1.4
146	0.06576	0.19	0.028	2.6
160	0.00848	0.28	0.059	5.5
165	0.58739	0.06	0.011	1.0
166	0.27845	0.13	0.020	1.8
167	0.36520	0.12	0.021	2.0
168	0.22595	-0.18	-0.026	-2.4
169	0.00218	0.57	0.074	6.8
170	0.71165	-0.06	-0.009	-0.8
171	0.00303	-0.44	-0.031	-2.9
175	0.08875	-0.25	-0.025	-2.3
187	0.00085	0.39	0.059	5.4
188	0.43330	0.12	0.008	0.7
189	0.00061	0.33	0.084	7.7
190	0.00004	0.44	0.062	5.7
191	0.00757	0.26	0.027	2.5
192	0.12728	0.16	0.044	4.0
193	0.86099	0.02	0.003	0.3
194	0.49989	0.09	0.015	1.4
215	0.43426	-0.10	-0.006	-0.5
216	0.93496	0.01	0.001	0.1
217	0.00064	-0.38	-0.047	-4.3
218	0.58538	0.06	0.010	0.9
219	0.08877	0.21	0.026	2.4
220	0.89510	-0.02	-0.010	-1.0
221	0.33676	0.12	0.013	1.2
226	0.03561	0.23	0.023	2.1

Plot ID	p value	Kendall's τ	Theil-Sen's slope	Seasonal change (%)
241	0.01996	0.26	0.040	3.6
242	0.89854	-0.02	-0.001	0.0
243	0.00214	0.33	0.065	5.9
245	0.37990	0.10	0.011	1.0
246	0.32236	0.14	0.021	1.9
248	0.01925	-0.39	-0.060	-5.5
255	0.90654	-0.02	-0.005	-0.4
269	0.58623	0.09	0.013	1.2
270	0.03557	0.24	0.035	3.2
271	0.30117	0.14	0.024	2.2
272	0.22157	0.12	0.022	2.0
273	0.68938	-0.07	-0.016	-1.5
274	0.31230	-0.17	-0.060	-5.5
275	0.60222	-0.08	-0.011	-1.0
295	0.22107	0.14	0.034	3.1
297	0.46745	0.07	0.010	0.9
298	0.22518	-0.16	-0.044	-4.0
299	0.90341	-0.02	-0.002	-0.2
300	0.64646	-0.06	-0.012	-1.1
301	0.23379	0.14	0.026	2.4
302	0.25970	-0.17	-0.020	-1.9
303	0.73494	-0.06	-0.009	-0.8
307	0.77466	0.05	0.011	1.0
329	0.02465	-0.36	-0.035	-3.3
341	0.14689	0.12	0.004	0.4
347	0.90653	-0.02	-0.002	-0.2
378	0.23631	0.21	0.036	3.3
384	0.35964	-0.12	-0.007	-0.7
385	0.00000	0.52	0.062	5.7
401	0.80264	0.04	0.005	0.5
402	0.00000	0.54	0.111	10.2
409	0.08000	-0.24	-0.024	-2.2
418	0.43978	0.10	0.021	1.9
419	0.20376	0.17	0.018	1.7
420	0.03442	0.27	0.020	1.8
460	0.00726	-0.37	-0.027	-2.5
464	0.58583	-0.08	-0.006	-0.6
468	0.13493	-0.23	-0.041	-3.8
475	0.54698	-0.08	-0.019	-1.8
485	0.47148	-0.12	-0.007	-0.6
500	0.00797	-0.58	-0.091	-8.4

REFERENCES

- Ågren, A. M., Larson, J., Paul, S. S., Laudon, H., and Lidberg, W.: Use of multiple LIDAR-derived digital terrain indices and machine learning for high-resolution national-scale soil moisture mapping of the Swedish forest landscape, Geoderma, 404, 115280, https://doi.org/10.1016/j.geoderma.2021.115280, 2021.
- Beven, K. J. and Kirkby, M. J.: A physically based, variable contributing area model of basin hydrology / Un modèle à base physique de zone d'appel variable de l'hydrologie du bassin versant, Hydrological Sciences Bulletin, 24, 43–69, https://doi.org/10.1080/02626667909491834, 1979.
- Buchanan, B. P., Fleming, M., Schneider, R. L., Richards, B. K., Archibald, J., Qiu, Z., and Walter, M. T.: Evaluating topographic wetness indices across central New York agricultural landscapes, Hydrology and Earth System Sciences, 18, 3279–3299, https://doi.org/10.5194/hess-18-3279-2014, 2014.
- Chianucci, F. and Macek, M.: hemispheR: an R package for fisheye canopy image analysis, Agricultural and Forest Meteorology, 336, 109470, https://doi.org/10.1016/j.agrformet.2023.109470, 2023.
- Esri Inc.: ArcGIS Pro, Version 3.1.1, 2023.
- Hägglund, B. and Lundmark, J.-E.: Skattning av höjdboniteten med ståndortsfaktorer: tall och gran i Sverige, Institutionen för växtekologi och marklära, Skogshögskolan, Stockholm, Sweden, 240 pp., 1977.
- Hjerdt, K. N., McDonnell, J. J., Seibert, J., and Rodhe, A.: A new topographic index to quantify downslope controls on local drainage, Water Resources Research, 40, https://doi.org/10.1029/2004WR003130, 2004.
- IUSS (International Union of Soil Sciences) and FAO (Food and Agriculture Organization of the United Nations): World reference base for soil resources 2014 International soil classification system for naming soils and creating legends for soil maps Update 2015, 1st ed., FAO, Rome, Italy, 203 pp., 2015.
- Lantmäteriet: Orthophoto [dataset], https://www.lantmateriet.se/globalassets/geodata/geodataprodukter/flyg--och-satellitbilder/e pb ortofoto.pdf, last access: 20 August 2024, 2021.
- Lantmäteriet: Swedish Property Map, scale 1:10000 [map], https://www.lantmateriet.se/globalassets/geodata/geodataprodukter/topografi_10_nedladdning_vektor.pdf, last access: 20 August 2024, 2023.
- Larson, J., Lidberg, W., Ågren, A. M., and Laudon, H.: Predicting soil moisture conditions across a heterogeneous boreal catchment using terrain indices, Hydrology and Earth System Sciences, 26, 4837–4851, https://doi.org/10.5194/hess-26-4837-2022, 2022.
- Larson, J., Wallerman, J., Peichl, M., and Laudon, H.: Soil moisture controls the partitioning of carbon stocks across a managed boreal forest landscape, Sci Rep, 13, 14909, https://doi.org/10.1038/s41598-023-42091-4, 2023.
- Lidberg, W., Nilsson, M., Lundmark, T., and Ågren, A. M.: Evaluating preprocessing methods of digital elevation models for hydrological modelling, Hydrological Processes, 31, 4660–4668, https://doi.org/10.1002/hyp.11385, 2017.
- Lindsay, J. B.: Efficient hybrid breaching-filling sink removal methods for flow path enforcement in digital elevation models, Hydrological Processes, 30, 846–857, https://doi.org/10.1002/hyp.10648, 2016.

- Marklund, L. G.: Biomass functions for pine, spruce and birch in Sweden, Report 45, Swedish University of Agricultural Sciences, Department of Forest Survey, 73 pp., ISSN 0348-0496, 1988.
- Meles, M. B., Younger, S. E., Jackson, C. R., Du, E., and Drover, D.: Wetness index based on landscape position and topography (WILT): Modifying TWI to reflect landscape position, Journal of Environmental Management, 255, 109863, https://doi.org/10.1016/j.jenvman.2019.109863, 2020.
- Muñoz-Sabater, J.: ERA5-Land hourly data from 1950 to present, Copernicus Climate Change Service (C3S) Climate Data Store (CDS) [dataset], https://doi.org/10.24381/cds.e2161bac, last access: 3 December 2024, 2019.
- Murphy, P. N. C., Ogilvie, J., Castonguay, M., Zhang, C., Meng, F.-R., and Arp, P. A.: Improving forest operations planning through high-resolution flow-channel and wet-areas mapping, The Forestry Chronicle, 84, 568–574, https://doi.org/10.5558/tfc84568-4, 2008.
- Naturvårdsverket: The National Land Cover database: soil moisture index map, spatial resolution: 10×10 m, Swedish Environmental Protection Agency [map], https://geodatakatalogen.naturvardsverket.se/geonetwork/srv/swe/catalog.search#/metadata/cae71f45-b463-447f-804f-2847869b19b0, last access: 5 September 2024, 2022.
- Newman, D. R., Lindsay, J. B., and Cockburn, J. M. H.: Evaluating metrics of local topographic position for multiscale geomorphometric analysis, Geomorphology, 312, 40–50, https://doi.org/10.1016/j.geomorph.2018.04.003, 2018.
- Nilsson, M., Nordkvist, K., Jonzén, J., Lindgren, N., Axensten, P., Wallerman, J., Egberth, M., Larsson, S., Nilsson, L., Eriksson, J., and Olsson, H.: A nationwide forest attribute map of Sweden predicted using airborne laser scanning data and field data from the National Forest Inventory, Remote Sensing of Environment, 194, 447–454, https://doi.org/10.1016/j.rse.2016.10.022, 2017.
- Peichl, M., Nilsson, M., Smith, P., Marklund, P., De Simon, G., Löfvenius, P., Dignam, R., Holst, J., Mölder, M., Andersson, T., Kozii, N., Larmanou, E., Linderson, M., and Ottosson-Löfvenius, M.: ETC L2 Meteo, Svartberget, 2018-12-31–2023-12-31, ICOS RI [dataset], https://hdl.handle.net/11676/kF7lHD8qztNl_5HdsSPWUmHs, last access: 20 May 2024, 2024.
- Rennó, C. D., Nobre, A. D., Cuartas, L. A., Soares, J. V., Hodnett, M. G., Tomasella, J., and Waterloo, M. J.: HAND, a new terrain descriptor using SRTM-DEM: Mapping terra-firme rainforest environments in Amazonia, Remote Sensing of Environment, 112, 3469–3481, https://doi.org/10.1016/j.rse.2008.03.018, 2008.
- Seibert, J. and McGlynn, B. L.: A new triangular multiple flow direction algorithm for computing upslope areas from gridded digital elevation models, Water Resources Research, 43, https://doi.org/10.1029/2006WR005128, 2007.
- SGU (Sveriges geologiska undersökning): Soil depth map, spatial resolution: 10×10 m [map], https://resource.sgu.se/dokument/produkter/jorddjupsmodell-beskrivning.pdf, last access: 20 August 2024a, 2024.
- SGU (Sveriges geologiska undersökning): Soil types map, scale 1:25000 [map], https://resource.sgu.se/dokument/produkter/jordarter-25-100000-beskrivning.pdf, last access: 20 August 2024b, 2024.
- Skogsstyrelsen: Utförda avverkningar (clearcuts carried out) [dataset], https://geodpags.skogsstyrelsen.se/geodataport/feeds/UtfordAvverk.xml, last access: 2 April 2025, 2024.

- SLU (Sveriges lantbruksuniversitet): SLU Forest Map, spatial resolution: 25×25 m, Department of Forest Resource Management [map], https://www.slu.se/en/Collaborative-Centres-and-Projects/the-swedish-national-forest-inventory/foreststatistics/slu-forest-map/, last access: 7 April 2025, 2010.
- SLU (Sveriges lantbruksuniversitet): Field work instructions Swedish National Forest Inventory and Swedish Soil Inventory, Department of Forest Resource Management and Department of Soil and Environment, Umeå & Uppsala, Sweden, https://www.slu.se/globalassets/ew/org/centrb/rt/dokument/faltinst/nfi_fieldwork_instructions_eng.pdf, last access: 7 September 2024a, 2021.
- SLU (Sveriges lantbruksuniversitet): SLU Soil Moisture Map, spatial resolution: 2×2 m, Department of Forest Ecology and Management [map], https://www.slu.se/en/departments/forest-ecology-management/forskning/soil-moisture-maps/, last access: 8 April 2025b, 2021.
- Svartberget Research Station: Meteorological data from Stortjärn, platform, 2016-07-02–2022-11-22, Swedish Infrastructure for Ecosystem Science (SITES) [dataset], https://meta.fieldsites.se/objects/SwldWWD0fJ6VII7VCCrGknQT, last access: 20 May 2024a, 2022.
- Svartberget Research Station: Meteorological data from Svartberget, Åheden AWS, 2022, Swedish Infrastructure for Ecosystem Science (SITES) [dataset], https://hdl.handle.net/11676.1/v0bn_ufBJ4vgq8Nen9d-Vqe5, last access: 20 May 2024b, 2022.
- Svartberget Research Station: Meteorological data from Svartberget, Hygget AWS, 2022, Swedish Infrastructure for Ecosystem Science (SITES) [dataset], https://hdl.handle.net/11676.1/ztFYjWV-ljPFra7V0z7NKHvg, last access: 20 May 2024c, 2022.
- Tarboton, D. G.: A new method for the determination of flow directions and upslope areas in grid digital elevation models, Water Resources Research, 33, 309–319, https://doi.org/10.1029/96WR03137, 1997.
- USGS (U.S. Geological Survey): Landsat 8 Operational Land Imager (OLI) and Thermal Infrared Sensor (TIRS), Level 2 Science Product (Surface Reflectance), Path 194, Row 015, Collection 2, Tier 1, acquired on 2022-08-26 [dataset], https://earthexplorer.usgs.gov/, last access: 16 September 2024, 2022.
- Vermote, E., Justice, C., Claverie, M., and Franch, B.: Preliminary analysis of the performance of the Landsat 8/OLI land surface reflectance product, Remote Sensing of Environment, 185, 46–56, https://doi.org/10.1016/j.rse.2016.04.008, 2016.
- Wallerman, J., Axensten, P., Egberth, M., Janzén, J., Sandström, E., Fransson, J. E. S., and Nilsson, M.: SLU Forest Map Mapping Swedish Forests Since Year 2000, in: IGARSS 2021 IEEE International Geoscience and Remote Sensing Symposium, Brussels, Belgium, 6056–6059, https://doi.org/10.1109/IGARSS47720.2021.9554458, 2021.
- Wilson, J. P. and Gallant, J. C.: Terrain Analysis: Principles and Applications, John Wiley & Sons, New York, USA, 522 pp., 2000.